OPEN ACCESS

Single-file water as a one-dimensional Ising model

New Journal of Physics
The open-access journal for physics

Single-file water as a one-dimensional Ising model

Jürgen Köfinger[1,3] **and Christoph Dellago**[2]

[1] Laboratory of Chemical Physics, Bldg 5, National Institute of Diabetes and Digestive and Kidney Diseases, National Institutes of Health, Bethesda, MD 20892, USA

[2] Faculty of Physics, University of Vienna, Boltzmanngasse 5, 1090 Vienna, Austria

E-mail: koefingerj@mail.nih.gov

New Journal of Physics **12** (2010) 093044 (17pp)
Received 30 March 2010
Published 27 September 2010
Online at http://www.njp.org/
doi:10.1088/1367-2630/12/9/093044

Abstract. We show that single-file water in nanopores can be viewed as a one-dimensional (1D) Ising model, and we investigate, on the basis of this, the static dielectric response of a chain of hydrogen-bonded water molecules to an external field. To achieve this, we use a recently developed dipole lattice model that accurately captures the free energetics of nanopore water. In this model, the total energy of the system can be expressed as the sum of the effective interactions of chain ends and orientational defects. Neglecting these interactions, we essentially obtain the 1D Ising model, which allows us to derive analytical expressions for the free energy as a function of the total dipole moment and for the dielectric susceptibility. Our expressions, which agree very well with simulation results, provide the basis for the interpretation of future dielectric spectroscopy experiments on water-filled nanopore membranes.

[3] Author to whom any correspondence should be addressed.

Contents

1. Introduction

Water confined to hydrophobic, sub-nanometre channels forms single-file chains in which each water molecule is hydrogen-bonded to its nearest neighbours [1]. Such chains occur, for instance, in the cavities of transmembrane proteins in biological cells, where they play an important role in the transport of ions through the cell membrane [2]–[5]. Similar quasi-1D confinement can also be realized by carbon or boron-nitride nanotubes [1, 6], providing promising building blocks for future filtration devices [7]–[9], fuel cells [10]–[13] and sensing devices [14]. An important step towards the realization of these applications was recently made by Cambré *et al* [15], who observed for the first time that carbon nanotubes fill with water down to sub-nanometre diameters. While their work demonstrates that narrow carbon nanotubes indeed fill with water, experimental verification of the single-file structure inside the pores as predicted by simulations is still lacking.

At room temperature and atmospheric pressure, water in sufficiently narrow carbon nanotubes forms essentially continuous chains of dipolarly ordered water molecules connected by hydrogen bonds [1, 13]. Flips of the orientation of such chains occur rarely via the diffusion of a defect with anomalous hydrogen-bonding [11, 16]. For tubes longer than about 0.1 mm, this macroscopic order is destroyed by orientational defects, which act as domain walls between dipole-ordered segments of opposite direction. Theoretical and computational investigations of such nanopore water are facilitated by a recently developed dipole lattice model, which accurately captures the free energetics and dynamics of this system [11, 13, 17]. A particularly convenient formulation of the model, the charge picture, in which the energy is expressed as the sum of Coulomb-like interactions between defects and chain ends, permits us to carry out computer simulations of water-filled narrow pores from nanoscopic to macroscopic lengths and spanning multiple time scales [14]. Using this model, we have recently shown how these unique ordering properties of nanoconfined water can be probed experimentally by dielectric

spectroscopy and how the excitation energy, the diffusion constant and the effective interaction of defects can be deduced from such measurements [14].

The thermodynamic and kinetic properties of the model become particularly simple if the distance between the effective charges located at defect sites and at the chain ends is large such that their Coulomb-like interactions can be neglected [17]. Under such conditions, defects are uncorrelated, drastically simplifying the calculation of the ordering properties [13] and of the dielectric response of nanopore water [14]. Here, we show that in this case, single-file water can be described as a 1D Ising model, in which domain walls play the role of the orientational defects occurring in the water chain. Exploiting this analogy, we determine analytically the free energy as a function of the total dipole moment of a single-file water chain, and use this result to investigate the response of a chain to an external homogeneous electric field in the direction of the pore axis. We derive an analytical expression for the dielectric susceptibility of nanopore water, which can be used to make contact with dielectric spectroscopy experiments and implies that susceptibilities of systems at different temperatures or sizes are related to each other by a law of corresponding states. Computer simulations carried out without making the approximation of uncorrelated defects confirm all of our results.

The remainder of this paper is organized as follows. In section 2, we introduce the dipole lattice model and discuss under what conditions it reduces to the 1D Ising model. We then show that nanopore water is well described by a system of uncorrelated defects and defect pairs in section 3. An analytical expression for the total dipole moment distribution is derived in section 4 and used in section 5 to investigate the response to an external field. We end with some conclusions in section 6.

2. From the dipole model to the Ising model

A single-file chain of water molecules in a narrow pore consists of one or more ordered segments, or domains, in which the dipole moments of all water molecules point approximately in the same direction. In these segments, each water molecule donates a hydrogen bond to a water molecule on one side and accepts one from a molecule on the other side. Segments of opposite orientation are connected by orientational defects, water molecules with anomalous hydrogen-bonding. There are two types of defect, named L-defects and D-defects, alluding to the orientational defects occurring in hexagonal ice [11, 13]. Whereas the L-defect molecule donates two hydrogen bonds without accepting any, the D-defect molecule accepts two hydrogen bonds without donating any. A single-file water chain containing both an L-defect and a D-defect is shown schematically in figure 1(a).

2.1. The dipole lattice model

The free energetics of single-file water are well described by a recently developed dipole lattice model [17]. This model, in which point dipoles are arranged on a 1D lattice with regular spacing a, as depicted in figure 1(b), reproduces the filling/emptying of a pore as well as the ordering properties of the pore very accurately [13]. In the present paper, we consider only pores that are completely filled, i.e. the water molecules form a continuous chain without gaps. In this case, all N lattice sites are occupied by a dipole of magnitude μ, which is either parallel to the pore axis for water molecules within ordered segments or orthogonal to it for defect molecules. The

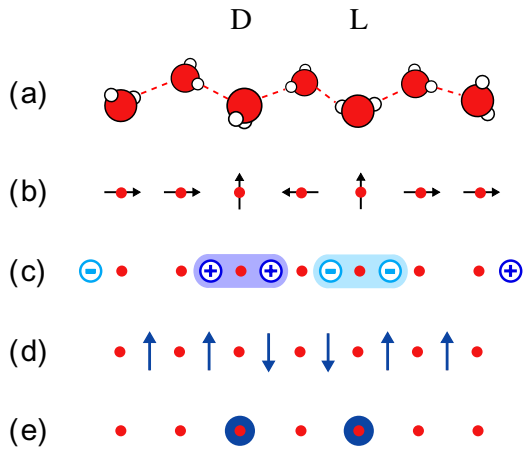

Figure 1. A single chain of water molecules containing two defects separated by a single molecule, i.e. a defect pair. (a) Whereas the D-defect molecule accepts two hydrogen bonds (dashed lines) without donating any, the L-defect molecule donates two bonds without accepting any. (b) In the dipole model, each molecule is represented by a dipole (arrow) on a lattice site (full circle). (c) In the charge representation, defects carry two charges and chain ends carry a single charge. A defect pair is represented by two kinks separated by two parallel spins in the 1D Ising model (d), which is isomorphic to a system of uncorrelated defects (large discs) (e).

energy of a particular configuration of dipoles is then given by the sum of all dipole–dipole interactions, leading to the Hamiltonian

$$H = -\sum_{i=1}^{N-1} \sum_{j=i+1}^{N} \frac{2 s_i s_j}{|j-i|^3}, \tag{1}$$

where the discrete spin-like variable s_i specifies the orientation of dipole i. Whereas $s_i = \pm 1$ for dipoles in ordered segments, defect dipoles orthogonal to the pore axis are assigned $s_i = 0$, because the interactions of the defect dipoles with other dipoles in the chain are negligible. The energy of the hydrogen bonds between adjacent water molecules is not taken into account explicitly in the above Hamiltonian, because the total number of hydrogen bonds is not changed by the formation of defects such that the total energy due to hydrogen bonding is the same for all configurations. Here and in the following, energy is measured in units of $\epsilon = \mu^2/(4\pi\varepsilon_0 a^3)$, where ε_0 is the vacuum permittivity.

It has been shown rigorously that 1D systems only display a true order–disorder transition if the interaction decays more slowly than $1/r^2$ with distance [18, 19]. Hence, similar to other 1D models with short-ranged interactions [20], the dipole model defined above is disordered in the thermodynamic limit at all finite temperatures because of the finite energy and the entropic benefit of the defects that destroy the order. As the temperature approaches $T = 0$, defects become rarer such that the correlation length grows exponentially but remains finite at all temperatures $T > 0$. As a consequence, no non-trivial critical behaviour is observed in the 1D dipole model.

2.2. Charge picture

In the mathematically equivalent charge picture of the dipole model, illustrated in figure 1(c), the total energy is written as the sum of interactions of effective charges carried by defects and chain ends. This charge picture is not only physically transparent and appealing, but also computationally very efficient and a useful basis for theoretical considerations. In the charge picture, the Hamiltonian is given by

$$H = \sum_{m=1}^{2n_\mathrm{d}+1} {\sum_{n=m+1}^{2n_\mathrm{d}+2}}' q_m q_n \Phi(|x_m - x_n|) + n_\mathrm{d} E_\mathrm{d}, \tag{2}$$

where n_d is the total number of defects, $E_\mathrm{d} = \zeta(2) - 1$ the defect excitation energy and $\zeta(x)$ is Riemann's zeta function [21]. The effective charges of magnitude $q_m = \pm 1$ are located at positions x_m at the endpoints of dipole-ordered segments and interact via

$$\Phi(x) = 2\Psi'(x) + z\Psi''(x) \approx \frac{1}{x}. \tag{3}$$

Here, $\Psi'(x)$ and $\Psi''(x)$ are polygamma functions [21]. For distances x larger than one lattice spacing, the interaction of effective charges is practically indistinguishable from the Coulombic $1/x$ interaction. Since in the charge picture effective charges are located at the endpoints of ordered segments, defects carry two of these charges and chain endpoints only one. The sign of the effective charges depends on the orientation of the corresponding ordered segments. Whereas D-defects carry a positive effective charge, the charge of L-defects is negative but of equal magnitude. Thus, defects of the same type repel each other, while defects of opposite type attract each other. Note that the prime next to the sum sign in (2) indicates that we do not include the interaction of the two charges forming a defect in this sum, because this contribution is incorporated into the defect excitation energy E_d. The parameters of the effective Hamiltonian can be obtained from molecular simulations carried out at room temperature and atmospheric pressure, yielding the values $a = 0.265\,\mathrm{nm}$ and $\mu = 1.9975\,\mathrm{D}$ for the lattice spacing and the magnitude of the dipole moment, respectively [13]. For these parameters, the effective defect charges have a magnitude of $2\mu/a \approx 0.31e$ and chain endpoints carry charges of half this magnitude.

Using a related but different approach to our derivation of the charge picture, Cardy [22] has shown that the effective interaction between domain walls in a 1D spin model has a logarithmic distance dependence if pairs of spins interact as $1/r^2$. In contrast to water in nanopores, where there is no phase transition in the thermodynamic limit, such a system displays a Kosterlitz–Thouless-like transition due to the logarithmic interaction of the defects [23].

2.3. The Ising model

Useful approximations of the effective Hamiltonian can be derived by neglecting most or all of the Coulomb interactions between the effective charges carried by defects and chain ends [17]. These simplified models were used in previous work for the investigation of the filling transition and helped to clarify the influence of the Coulomb interactions on the structural and thermodynamic behaviour of nanopore water [17].

Here, we go one step further and map all defect configurations onto the configurations of a 1D Ising model, in which spins are located between the sites of the dipole lattice model (see figure 1(d)). In this analogy, the orientational defects of the dipole model correspond to

the kinks of the 1D Ising model located between spins of opposite direction. Consequently, a chain with N molecules corresponds to an Ising model with $N-1$ sites, a difference in size that can be neglected for long chains. This particular mapping automatically takes into account that defects cannot be located at chain ends. The constraint that defects have to be separated by a single molecule implies that kinks in the Ising system are always separated by at least two spins. This is the case for the defect pair shown in figure 1, for example. The Hamiltonian of the Ising model is then given by

$$H = n_{\mathrm{d}} E_{\mathrm{d}}, \tag{4}$$

where the defect number n_{d} corresponds to the number of kinks. The defect excitation energy E_{d} is the energy needed to introduce a kink, $E_{\mathrm{d}} = 2J$, where J is the Ising coupling constant.

The relation of the total dipole moment along the pore axis of the dipole lattice model to the magnetization of the Ising model is complicated by the fact that a defect is located on a molecule with a dipole moment orthogonal to the axis. Consequently, the generation of a defect at a chain end changes the total dipole moment by $\pm 3\mu$, while the hop of a defect to an adjacent site changes it by only $\pm 2\mu$. In contrast, both the generation and the hop of a kink in the Ising model change the magnetization by ± 2 times the magnetic moment of a single spin. Thus, a one-to-one correspondence between the magnetization and the total dipole moment cannot be established. Nevertheless, for long chains, these complications can be either neglected or easily accounted for, as we shall see below.

If we not only neglect all Coulomb-like interactions but also ignore the configurational constraints of the model, which prevent adjacent defects and defects next to chain ends, we obtain a system of completely uncorrelated defects (figure 1(e)). This approximation is justified if the distances between defects (and endpoints) are typically large, i.e. if the defect number is small compared to the number of molecules in the chain. Every site of the lattice can then be occupied by either zero defects or one defect, each of which contributes the defect energy E_{d} to the total energy of the system. In this simplified model, we have to account for the degeneracy of states due to the two possible orientations of the chain, which then renders this model exactly isomorphic to the 1D Ising model.

3. Uncorrelated defects and defect pairs

The success of approximations in which most or all of the charges are neglected raises the question: to what extent can a chain of water molecules be described by a system of completely uncorrelated defects? In the following, we will inspect the validity of this approximation, which underlies the analogy with the Ising model.

3.1. Uncorrelated defects

Collecting states with the same number of defects and noting that the number of distinct configurations with n_{d} defects is given by the binomial coefficient $\binom{N}{n_{\mathrm{d}}}$, one can rewrite the partition function of a gas of completely uncorrelated defects as

$$Z_{\mathrm{s}}(\beta, N) = 2 \sum_{n_{\mathrm{d}}=0}^{N} \binom{N}{n_{\mathrm{d}}} \mathrm{e}^{-\beta E_{\mathrm{d}} n_{\mathrm{d}}}, \tag{5}$$

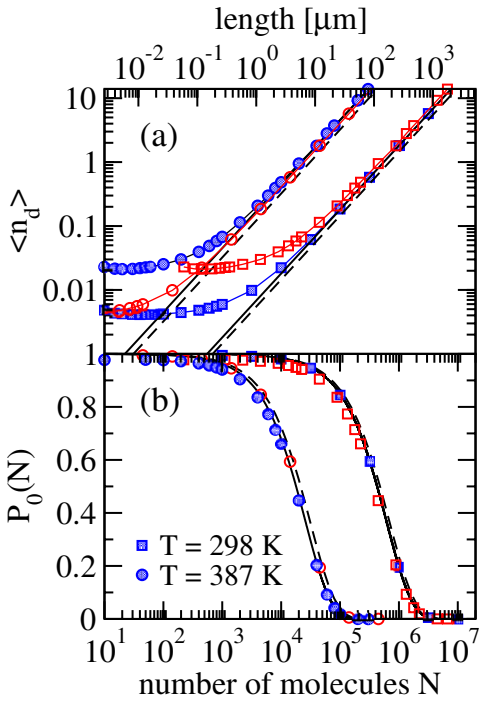

Figure 2. Average defect number $\langle n_\mathrm{d}\rangle$ (a) and order probability $P_0(N)$ (b). Simulation results are depicted as full symbols which are connected by thin lines for $\langle n_\mathrm{d}\rangle$. The approximation of uncorrelated defects is shown as dashed lines and the approximation of uncorrelated defects and defect pairs as solid lines. Open symbols indicate rescaled simulation results obtained using the law of corresponding states given by (15).

where the factor of 2 on the right-hand side takes into account the symmetry of the original model with respect to dipole inversion. Using the binomial identity, one obtains

$$Z_\mathrm{s}(\beta, N) = 2(1+\mathrm{e}^{-\beta E_\mathrm{d}})^N. \tag{6}$$

In the following, we will use this expression to derive expressions for various properties of the model and compare them with numerical results.

According to (5), the average defect number $\langle n_\mathrm{d}\rangle$ is given by

$$\langle n_\mathrm{d}\rangle = -\frac{1}{Z_\mathrm{s}(\beta, N)}\frac{\partial Z_\mathrm{s}(\beta, N)}{\partial(\beta E_\mathrm{d})} = N\frac{\mathrm{e}^{-\beta E_\mathrm{d}}}{1+\mathrm{e}^{-\beta E_\mathrm{d}}}. \tag{7}$$

In figure 2(a), we compare this analytical expression with simulation results determined in Monte Carlo simulations using the full Hamiltonian (2). For long chains, the system of uncorrelated defects qualitatively reproduces the simulation results, but the results are shifted by a constant on the logarithmic scale to lower values. As explained later in this section, this offset is due to the neglect of defect pairs, which have an excitation energy only slightly higher than that of single defects. For short chains, on the other hand, the defect number obtained in the simulations deviates considerably from the straight line expected for uncorrelated defects. The reason for this behaviour is that a single defect in an otherwise ordered chain interacts

attractively with the effective charges at the chain ends. This interaction, which is neglected in the uncorrelated defect model, lowers the free energy required to create a defect and therefore increases the defect density. The interplay between the increase in entropy and the decrease in the influence of the chain ends with increasing system size even leads to the formation of shallow minima in the defect number at $N \approx 40$ and 20 for temperatures $T = 298$ and 387 K, respectively.

Similar behaviour is observed for the order probability $P_0(N)$, i.e. the probability that the system is free of defects. This probability is obtained as the number of ordered states divided by the partition function, i.e.

$$P_0(N) = \frac{2}{Z_s(\beta, N)} = (1 + e^{-\beta E_d})^{-N}. \tag{8}$$

As shown in figure 2(b), this approximation slightly overestimates the order probability compared to the results for the full Hamiltonian. For long chains, the difference between simulation results and the approximation of uncorrelated defects can be attributed to the occurrence of defect pairs, as we shall see in the following.

3.2. Uncorrelated defect pairs

A defect pair consists of an L- and a D-defect separated by a single molecule (see figure 1(a)). In contrast to single defects, which form at chain ends, defect pairs can form anywhere within ordered segments. The generation of a defect pair within an ordered segment changes the total dipole moment by $-4\,s\mu$ independently of its position within the segment. Here, s denotes the orientation of the ordered segment and can take the values +1 and −1. Since in the charge picture the L- and the D-defect consist of charges with equal magnitude but opposite sign, a defect pair is charge neutral and forms an effective dipole aligned with the chain. As a consequence, the interaction of a defect pair with other effective charges decays rapidly with distance.

The excitation energy of a defect pair far from other effective charges is given by the sum of twice the defect excitation energy E_d and the interaction energy of the two defects with each other,

$$E_p = 2E_d - \Phi(1) - 2\Phi(2) - \Phi(3), \tag{9}$$

where $\Phi(x)$ is the Coulomb-like interaction (3). Due to the strong interaction of the two defects forming the defect pair, the defect pair excitation energy is only about 15% larger than the excitation energy of a single defect. For a water-filled carbon nanotube at ambient conditions, the defect pair excitation energy is $\beta E_p \approx 15.55$, compared to $\beta E_d \approx 13.44$ for the excitation energy of a single defect.

Due to the high defect pair excitation energy E_p, the density of defect pairs is low, but it cannot be neglected with respect to the density of single defects. For large systems, one can safely assume that defect pairs are uncorrelated and independent of single defects. In this case, the partition function of a system of uncorrelated defect pairs, $Z_p(\beta, N)$, is given by

$$Z_p(\beta, N) = (1 + e^{-\beta E_p})^N, \tag{10}$$

resembling the form of the partition function of a system of individual uncorrelated defects given by (6). Thus, the partition function of a system of uncorrelated defects and defect pairs becomes

$$Z(\beta, N) = Z_s(\beta, N) Z_p(\beta, N). \tag{11}$$

The average defect number, including the defects occurring in defect pairs, is then given by

$$\langle n_{\mathrm{d}}\rangle = -\frac{1}{Z(\beta, N)}\left[\frac{\partial Z(\beta, N)}{\partial(\beta E_{\mathrm{d}})} + 2\frac{\partial Z(\beta, N)}{\partial(\beta E_{\mathrm{p}})}\right], \tag{12}$$

such that

$$\langle n_{\mathrm{d}}\rangle/N = \frac{\mathrm{e}^{-\beta E_{\mathrm{d}}}}{1+\mathrm{e}^{-\beta E_{\mathrm{d}}}} + 2\frac{\mathrm{e}^{-\beta E_{\mathrm{p}}}}{1+\mathrm{e}^{-\beta E_{\mathrm{p}}}}. \tag{13}$$

This analytical result agrees well with the simulation results shown in figure 2(a) for $N \gtrsim 10^4$. Taking into account defect pairs, the order probability becomes

$$P_0(N) \approx \frac{2}{Z(\beta, N)} = [(1+\mathrm{e}^{-\beta E_{\mathrm{d}}})(1+\mathrm{e}^{-\beta E_{\mathrm{p}}})]^{-N}, \tag{14}$$

which is in excellent agreement with simulation results obtained for the full Hamiltonian, as shown in figure 2(b).

3.3. Corresponding states

For a system of uncorrelated defects with a large defect excitation energy, i.e. $b \equiv \mathrm{e}^{-\beta E_{\mathrm{d}}} \ll 1$, a law of corresponding states can be derived. To obtain this relation, which is useful to investigate systems that are too large for numerical simulations, we approximate the partition function as $Z_{\mathrm{s}}(\beta, N) \approx 2(1+Nb)$, the defect number as $\langle n_{\mathrm{d}}\rangle \approx Nb$ and the order probability as $P_0(N) \approx 1 - Nb$. These expressions agree well with simulation results, and they depend on the system size and the temperature only through the average defect number Nb. Note that b is the inverse of the average domain length l. Thus, from the point of view of thermodynamics, a system of size N at an inverse temperature β can be viewed as a coarse-grained description of a larger system with size N', an inverse temperature β' and a defect excitation energy E'_{d}, provided $Nb = N'b'$. This condition, requiring that the two systems have an equal average number of defects, is equivalent to the relation

$$\frac{N}{N'} = \mathrm{e}^{(\beta E_{\mathrm{d}} - \beta' E'_{\mathrm{d}})}, \tag{15}$$

which can be used to relate results obtained at one temperature to those obtained at another temperature, as shown in figure 2. Here, the horizontal axis was rescaled using (15), leading to a constant shift of the curves to the left when going from lower to higher temperatures. For sufficiently long chains, we obtain excellent agreement between the original and the rescaled data. Note that here we use the same values for the lattice spacing a and the dipole moment μ at both temperatures, resulting in $E_{\mathrm{d}} = E'_{\mathrm{d}}$. In general, these parameters depend on the temperature and thus the defect excitation energy is a function of T.

Therefore, for long water chains, the order probability and the average defect number are quantitatively reproduced by a system of uncorrelated defects and uncorrelated defect pairs. Using the analogy between such a system and the 1D Ising model, one can also derive an analytical expression for the free energy as a function of the total dipole moment, as we will do in the next section.

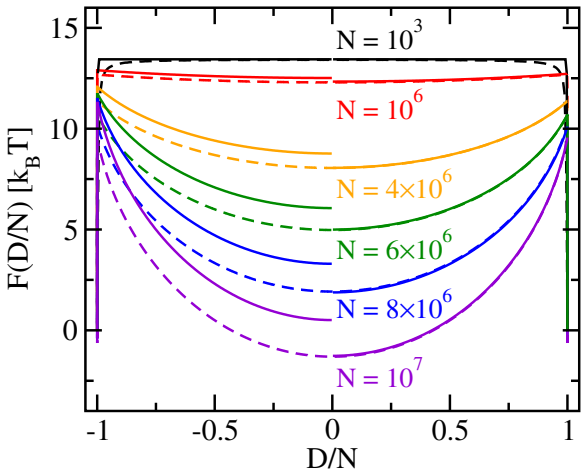

Figure 3. Free energy as a function of the total dipole moment per site. The curves are shifted so that the free energy of the ordered states vanishes. Dashed lines are simulation results for the full Hamiltonian. For negative values of the total dipole moment, we plot the free energy for uncorrelated defects, which have a higher free energy at vanishing dipole moment than the results for the full Hamiltonian. For positive values of the total dipole moment, we show results obtained including uncorrelated defect pairs, which agree well with the simulation results.

4. Total dipole moment distribution

Since the orientation of individual water molecules with respect to the pore axis can flip due to the formation and diffusion of thermally excited hydrogen bonding defects, the reduced total dipole moment $D = \sum_i s_i$, related to the total dipole moment M by $M = \mu D$, is a fluctuating quantity with a statistical distribution $P(D)$. From this distribution, the free energy $F(D) = -k_B T \ln P(D)$ follows. Free energy curves $F(D)$, shown in figure 3 as obtained from Monte Carlo simulations for the full Hamiltonian (dashed lines) [13], reflect the transition, with increasing system size, from a predominantly ordered system to a disordered system. For short chains, the free energy curves display two minima corresponding to the ordered states at $D/N = \pm 1$ separated by a high free-energy barrier with the maximum at $D/N = 0$, effectively forming a two-state system. For long chains, the free-energy curves exhibit a pronounced quadratic minimum for vanishing dipole moment with residual minima corresponding to the ordered states. For intermediate system sizes, we observe a crossover behaviour with two deep minima for the ordered states, and one shallow minimum for vanishing dipole moment. At all systems sizes, the free energy is symmetric with respect to $D = 0$ such that the total dipole moment vanishes on average.

We obtain an analytical expression for the free energy as a function of the total dipole moment using the analogy between hydrogen-bonding defects in the water chain and kinks (or domain walls) in the 1D Ising model. To do that, we follow Antal *et al* [24], who derived the partition function as a function of the magnetization of the 1D Ising model for various boundary conditions assuming a small kink density. Treating ordered and disordered states separately, we

obtain for the partition function for fixed reduced dipole moment D

$$Z_{\mathrm{N}}(D) = \begin{cases} 1 & \text{for } |D| = N, \\ \mathcal{Z}_N(D) = bI_0(by) + Nb\dfrac{I_1(by)}{y} & \text{else,} \end{cases} \tag{16}$$

where $I_i(x)$ are modified Bessel functions of the first kind [21] and $y = \sqrt{N^2 - D^2}$. The only difference compared to the corresponding expression for the Ising model is that in single-file water the possible values for odd and even defect numbers are different, which we can account for by a factor of $1/2$ in the expression for the partition function of disordered states of the Ising model [25]. The distribution of the total dipole moment is obtained as

$$P_N(D) = \frac{1}{Z_N} Z_N(D), \tag{17}$$

where

$$Z_N = 2 + \sum_{D=-N+3}^{N-3} \mathcal{Z}_N(D). \tag{18}$$

Consequently, the free energy as a function of the total dipole moment is given by

$$\beta F(D) = -\ln Z_N(D). \tag{19}$$

In the limit of long chains, the distribution of the total dipole moment is Gaussian and the free energy is parabolic, $\beta F(D) = -D^2/2Nl$, where we have omitted an irrelevant constant. Thus, the width of the Gaussian distribution, $\sigma = \sqrt{Nl}$, grows for increasing system size and average domain length $l = \mathrm{e}^{\beta E_{\mathrm{d}}}$.

In figure 3, we compare the free energy as a function of the total dipole moment obtained from simulations using the full Hamiltonian with the analytical expression for uncorrelated defects (19). Although the shape of the free energy for disordered states is captured by the approximation of uncorrelated, single defects, free energies are too high with respect to the ordered states. The reason is that uncorrelated defect pairs lead to a larger statistical weight of the disordered states in the partition function, i.e.

$$Z_{\mathrm{N}}(D) = \begin{cases} 1 & \text{for } |D| = N, \\ \mathcal{Z}_N(D)(1 + \mathrm{e}^{-\beta E_{\mathrm{p}}})^N & \text{else.} \end{cases} \tag{20}$$

Here, we have exploited the fact that the change in the total dipole moment due to the occurrence of defect pairs is small compared to the change due to different positions of single defects and can be neglected. The degeneracy of the disordered states arising from the extra entropy of the defect pairs results in a linear shift,

$$\beta F_{\mathrm{p}} = -\ln Z_{\mathrm{p}} = -N \ln(1 + \mathrm{e}^{-\beta E_{\mathrm{p}}}), \tag{21}$$

with respect to the free energy given by (19). Taking this shift into account, we obtain excellent agreement between simulations and theory, as shown in figure 3.

The shift F_{p} in the free energy is small for predominantly ordered systems with $\lesssim 10^5$ molecules (for example, for a larger system size of $N = 10^6$ the shift is only $\beta F_{\mathrm{p}} \approx 0.18$). Thus, the shift in the free energy can be neglected for short chains. For longer chains, the shift increases the statistical weight of the disordered states with respect to the ordered states. However, since the ordered states have a small statistical weight for long chains, this shift does not appreciably affect the thermodynamic behaviour. As a consequence, the degeneracy of the

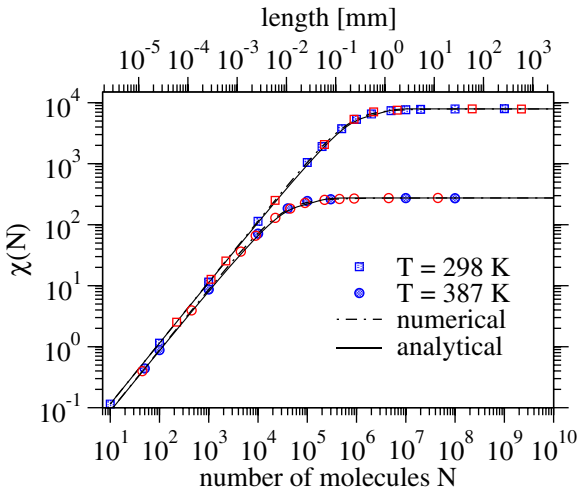

Figure 4. Static dielectric susceptibility $\chi(N)$ of a water-filled nanopore membrane at temperatures $T = 298$ and 387 K as obtained by numerical summation according to (26) (dash-dotted line) and analytically using the assumption of uncorrelated defects ((32), solid lines). The analytical and numerical curves are indistinguishable on the scale of the figure. Also shown are results of Monte Carlo simulations [14] for $T = 298$ K (full squares) and $T = 387$ K (full circles). Data rescaled according to the law of corresponding states given by (15) and (35) are shown as open symbols.

disordered states with respect to the ordered states can be neglected for most averages over the probability distribution function of the total dipole moment, such as the average total dipole moment or its fluctuations (see figure 4). Therefore, analytical results for the field dependence of these quantities derived for the 1D Ising model [26] are applicable to single-file water. In the following, we use the free energy as a function of the total dipole moment to investigate the response of the total dipole moment of nanopore water to a static external electric field.

5. Static dielectric response

In an electric field, the dipole moments tend to orient into the field direction. A homogeneous electric field E in the direction of the pore axis couples to the total dipole moment M of the water chain and leads to an electrostatic interaction energy $-DE_\mathrm{f}$, where $E_\mathrm{f} = E\mu/\epsilon$ is the reduced electric field. Consequently, the distribution function of the total dipole moment at field E_f can be obtained from the distribution function at vanishing field $P(D)$ via

$$P(D, E_\mathrm{f}) = \frac{P(D)\mathrm{e}^{\beta D E_\mathrm{f}}}{\sum_{\{D\}} P(D)\mathrm{e}^{\beta D E_\mathrm{f}}}, \tag{22}$$

where the sum is over all possible values of D. Since $\beta F(D, E_\mathrm{f}) = -\ln P(D, E_\mathrm{f})$ up to a constant depending on the field E_f, the free energy is given by

$$F(D, E_\mathrm{f}) = F(D) - DE_\mathrm{f}, \tag{23}$$

where $\beta F(D)$ is the free energy for a vanishing external field. Thus, the effect of an external homogeneous electric field in the direction of the pore axis is simply to tilt the free-energy

curves by $-DE_f$. We next use the results for $P(D)$ from Monte Carlo simulations and from the analytical expression given by (16) (see figure 3) and investigate the influence of the electric field on the total dipole moment of the chain.

5.1. Linear response

The linear response of the total dipole moment M of the water chain to an electric field, E, is quantified by the static dielectric susceptibility χ defined as

$$\chi = \frac{1}{\varepsilon_0 V} \left. \frac{\mathrm{d}\langle M \rangle}{\mathrm{d}E} \right|_{E=0}, \tag{24}$$

where the derivative is evaluated at $E = 0$ and angular brackets indicate a canonical ensemble average. In the above equation, V denotes the volume of the sample and $\langle M \rangle / V$ is the polarization. The susceptibility χ is related to the equilibrium fluctuations of the total dipole moment for vanishing electric field via the fluctuation-dissipation theorem [27],

$$\chi = \beta \frac{\langle M^2 \rangle}{\varepsilon_0 V}, \tag{25}$$

where we have taken into account that $\langle M \rangle = 0$. Since the susceptibility is defined for a bulk material of volume V, we will consider the susceptibility of a membrane with parallel pores with a given area density. For easier comparison with previous results [14], we will use a pore density of $2.5 \times 10^{11}\ \mathrm{cm}^{-2}$ corresponding to a volume per molecule of $v = 106\ \mathrm{nm}^3$. We assume that in this membrane the pores are sufficiently far apart such that water wires in adjacent pores are uncorrelated. Consequently, the static susceptibility of such a membrane is equal to that of a single pore with volume $V = Nv$.

Since the assumption of uncorrelated defects yields an excellent approximation for the total dipole moment (see figure 3), we can estimate the static susceptibility using the partition function $Z_N(D)$ for fixed D from (16). Expressing the average of the squared total dipole as

$$\langle M^2 \rangle = \frac{\sum_{\{D\}} \mu^2 D^2 Z_N(D)}{\sum_{\{D\}} Z_N(D)}, \tag{26}$$

and approximating the sums by integrals that we evaluate numerically, we calculate the dielectric susceptibility using (25). The results of this calculation agree very well with simulation results for both temperatures and all system sizes investigated here (see figure 4), confirming that defects are indeed uncorrelated to a large extent.

For uncorrelated defects, we also find a relation between the static dielectric susceptibilities of corresponding states. In the limit of large system sizes, the partition function for fixed total dipole moment D is given by a Gaussian distribution [24],

$$\tilde{\mathcal{Z}}_N(D) = \frac{2b\mathrm{e}^{bN}}{\sqrt{2\pi N b}} \mathrm{e}^{-D^2 b/2N}. \tag{27}$$

Approximating the sums by integrals yields

$$\langle D^2 \rangle = \frac{1}{\tilde{\mathcal{Z}}_N} \left(2N^2 + \int_{-N}^{N} \mathrm{d}D D^2 \tilde{\mathcal{Z}}_N(D) \right), \tag{28}$$

where

$$\tilde{\mathcal{Z}}_N = 2 + \int_{-N}^{N} \mathrm{d}D \tilde{\mathcal{Z}}_N(D). \tag{29}$$

Analytical integration of (28) and (29) then leads to

$$\langle D^2 \rangle = \frac{N}{b} G(bN), \tag{30}$$

where

$$G(y) = \frac{y - \mathrm{e}^{y/2}\sqrt{\frac{2y}{\pi}} + \mathrm{e}^{y}\mathrm{erf}\left(\sqrt{\frac{y}{2}}\right)}{\mathrm{e}^{y}\mathrm{erf}\left(\sqrt{\frac{y}{2}}\right) + 1}. \tag{31}$$

Here, $y = bN = \exp(-\beta E_\mathrm{d} + \ln(N))$ and $\mathrm{erf}(x)$ denotes the error function [21]. Thus, we obtain the following approximation for the dielectric susceptibility,

$$\chi(\beta, N) = \frac{\beta\mu^2}{\varepsilon_0 V}\frac{N}{b} G(bN). \tag{32}$$

This expression captures the static dielectric susceptibility for all system sizes to a good approximation (see figure 4). For short chains, the number of defects and, hence, y are small. The function $G(y)$ can then be approximated by $G(y) \approx y$, and we find, in agreement with results obtained for a two-state model [14],

$$\chi_\mathrm{short}(\beta, N) = \frac{\beta\mu^2}{\varepsilon_0 v} N. \tag{33}$$

This expression does not depend on the defect excitation energy and is a consequence of the two-state behaviour of the total dipole moment, which, in the presence of an external electric field, was confirmed by molecular dynamics simulations [28]. In this work [28], the authors apply a field of up to $\sim 10^9\ \mathrm{V\,m^{-1}}$ to a chain of five water molecules. They compare simulation results of the average value and the variance of the total dipole moment to predictions of a two-state model and find them in excellent agreement. Up to fields of $\sim 2 \times 10^8\ \mathrm{V\,m^{-1}}$, the average dipole moment of individual water molecules in the direction of the pore axis is essentially the same as in the field-free case. Only for larger field strengths do individual water molecules align into the field direction, leading to an appreciably larger component of the dipole moment along the axis.

For large values of y, corresponding to long chains, the function $G(y)$ converges to $G(y) \approx 1$ and the dielectric susceptibility is given by

$$\chi_\mathrm{long}(\beta, N) = \frac{\beta\mu^2}{\varepsilon_0 v} \mathrm{e}^{\beta E_\mathrm{d}}, \tag{34}$$

as expected from the analytical solution of the 1D Ising model in the thermodynamic limit [14, 26]. The crossover between this constant regime and the linear regime for short chains occurs at a chain length of about $\exp(-\beta E_\mathrm{d})$ at which there is one defect in the chain on average. Note that equation (34) for the susceptibility in the long chain limit can be obtained from the short chain expression (33) simply by replacing the chain length N by the average domain length $\exp(-\beta E_\mathrm{d})$.

The argument of the function $G(bN)$ in (32) has the same value for corresponding states with the same average number of defects, i.e. with $Nb = N'b'$. Since the volume V is proportional to the pore length (for a single pore as well as for a membrane with a given pore density), i.e. $V = vN$ and $V' = vN'$, we obtain a relation between the dielectric susceptibilities

of the two corresponding systems with dipole moments μ and μ' and excitation energies E_d and E'_d,

$$\frac{\chi(\beta, N)}{\chi(\beta', N')} = \frac{\beta\mu^2}{\beta'\mu'^2} \mathrm{e}^{(\beta E_\mathrm{d} - \beta' E'_\mathrm{d})}. \tag{35}$$

We used this relation to obtain estimates for the static dielectric susceptibility at $T = 298\,\mathrm{K}$ from simulations at $T = 387\,\mathrm{K}$, and the other way round, and found good agreement (see figure 4). Here, we again neglect the temperature dependence of the dipole moment and the excitation energy in our simulation, i.e. $\mu = \mu'$ and $E_\mathrm{d} = E'_\mathrm{d}$, for which (35) simplifies to $\chi(\beta, N)/\chi(\beta', N') = \exp[(\beta - \beta')E_\mathrm{d}]\beta/\beta'$.

The limiting cases given by (33) and (34) permit us to determine the average dipole moment of a water molecule along the pore axis, μ, and the defect excitation energy, E_d, from the linear increase of the dielectric susceptibility at small system sizes and its value in the thermodynamic limit, provided one knows the number of chain molecules $N = L/a$, where L is the length of the chain. Once the defect excitation at one specific temperature has been determined, the laws of corresponding states given by (15) and (35) can be applied, effectively decreasing the number of measurements needed to determine the dipole moment and the excitation energy at another temperature. Thus, dielectric spectroscopy experiments offer the possibility to provide useful information on the microscopic structure of 1D water chains in narrow pores.

Since for very strong electric fields all dipoles align with the field, the total dipole moment saturates as a function of the field strength, such that the linear relation between field strength and total dipole moment quantified by the susceptibility cannot remain valid for arbitrarily strong fields. The limit of the linear regime can be estimated in the following way. Linear response certainly breaks down at field strengths for which the value of the total dipole moment as expected from the value of the susceptibility, $\langle M\rangle = \varepsilon_0 V \chi E$, equals or exceeds the dipole moment at saturation, $\langle M\rangle = N\mu$. Equating these two expressions, one finds a critical field $E_\mathrm{c} = \mu N/\varepsilon_0 V\chi$, which can be regarded as an upper limit of the linear response regime. Inserting the expression of the susceptibility for short chains (33), one obtains $E_\mathrm{c} = k_\mathrm{B}T/N\mu$, implying that the critical field decreases for growing chain length. For long chains, insertion of the susceptibility from (34) yields $E_\mathrm{c} = k_\mathrm{B}T/\mathrm{e}^{\beta E_\mathrm{d}}\mu$. Thus, once the chain has reached a size of about $\mathrm{e}^{\beta E_\mathrm{d}}$, in which there is at least one defect in the chain on average, the critical field E_c ceases to be a function of the chain length.

6. Conclusion

In summary, we have shown that a single-file chain of water molecules at room temperature can be accurately described as a 1D Ising model. In this analogy, the domain walls (kinks) of the Ising model correspond to the hydrogen-bonding defects in the water chain. While in the Ising model, domain walls do not interact with each other, because only neighbouring spins are coupled, hydrogen-bonding defects interact via effective $1/r$ potentials. Nevertheless, the analogy between the Ising model and the water chain holds, because at ambient conditions hydrogen-bonding defects occur with low density such that their interactions can be neglected. As a consequence, hydrogen-bonding defects occurring in a 1D water chain are statistically uncorrelated just as their Ising model counterparts. Only for very short chains do the Coulomb interactions between defects and chain endpoints matter and lead to a defect density higher than

that of a gas of non-interacting defects. Consequently, appreciable deviations from Ising like behaviour are observed.

Based on the approximation of uncorrelated defects, we have derived explicit expressions for the defect density and the order probability. These expressions agree very well with the results of Monte Carlo simulations in which all interactions are included. The agreement is even better if the effects of pairs of hydrogen-bonding defects separated by a single water molecule are taken into account. Although these defect pairs provide the predominant mechanism for defect generation and recombination in long tubes, their occurrence can be neglected with respect to the static dielectric response of the system. Consequently, we were able to obtain an analytical expression for the length-dependent static susceptibility exploiting the relation to the Ising model. From this expression, we derived a law of corresponding states that relates the susceptibilities of systems of different sizes and temperatures with each other. This law offers an efficient way to determine the temperature dependence of the defect excitation energy in dielectric spectroscopy experiments.

The derivation of the relation to the 1D Ising model presented here should also be applicable to water in wider tubes, which exhibits polygonal water rings with ferro-electric-like order [29]–[31] akin to that of single-file water. Similar behaviour is also expected for other hydrogen-bond-forming molecules or molecules with permanent magnetic or dipolar moments. For example, it was recently shown in molecular simulations that acetonitrile forms dipole-ordered single-file chains similar to those of water [32]. This variety of substances is of great interest for the design of super-capacitors as exemplified here for single-file water in carbon nanotubes, where we find that the static susceptibility is about 100 times larger than that of bulk water, although the water density in the membrane is about 3000 times smaller than that in the bulk. Thus, water-filled nanopore membranes may serve as high-k dielectrics, e.g. for use in sensing devices [33, 34].

Our estimation of the susceptibility of water-filled membranes is based on the assumption that chains of water molecules in different pores are uncorrelated with each other. This assumption may be inaccurate if the distance between pores is sufficiently small, such that water chains in neighbouring pores interact with each other. Then, collective phase behaviour may set in, introducing strong correlations and stabilizing ordered phases. Such phase transitions and their effect on the dielectric behaviour of the material are a topic we are currently addressing in our research [35].

Acknowledgments

We thank Gerhard Hummer and Georg Menzl for useful discussions. We acknowledge support from the Austrian Science Fund (FWF) under grants P20942-N16 and W004 and from the University of Vienna through the Focus Research Area *Materials Science*. JK was supported by the Intramural Research Program of the NIH, NIDDK. The simulations presented in this paper were carried out on the Vienna Scientific Cluster (VSC).

References

[1] Hummer G, Rasaiah J C and Noworyta J P 2001 *Nature* **414** 188
[2] de Groot B L and Grubmüller H 2001 *Science* **294** 2353
[3] Hille B 2001 *Ion Channels of Excitable Membranes* 3rd edn (Sunderland, MA: Sinauer)

[4] Tajkhorshid E, Nollert P, Jensen M O, Miercke L J W, O'Connell J, Stroud R M and Schulten K 2002 *Science* **296** 525
[5] Zhu F and Schulten K 2003 *Biophys. J.* **85** 236
[6] Won C Y and Aluru N R 2007 *J. Am. Chem. Soc.* **129** 2748
[7] Kalra A, Garde S and Hummer G 2003 *Proc. Natl Acad. Sci. USA* **100** 10175
[8] Fornasiero F, Park H G, Holt J K, Stadermann M, Grigoropoulos C P, Noy A and Bakajin O 2008 *Proc. Natl Acad. Sci. USA* **105** 17250
[9] Corry B 2008 *J. Phys. Chem.* B **112** 1427
[10] Kreuer K D, Paddison S J, Spohr E and Schuster M 2004 *Chem. Rev.* **104** 4637
[11] Dellago C, Naor M M and Hummer G 2003 *Phys. Rev. Lett.* **90** 10590
[12] Dellago C and Hummer G 2006 *Phys. Rev. Lett.* **97** 245901
[13] Köfinger J, Hummer G and Dellago C 2008 *Proc. Natl Acad. Sci. USA* **105** 13218
[14] Köfinger J and Dellago C 2009 *Phys. Rev. Lett.* **103** 080601
[15] Cambré S, Schoeters B, Luyckx S, Goovaerts E and Wenseleers W 2010 *Phys. Rev. Lett.* **104** 207401
[16] Pomès R and Roux B 1998 *Biophys. J.* **75** 33
[17] Köfinger J, Hummer G and Dellago C 2009 *J. Chem. Phys.* **130** 154110
[18] Ruelle D 1968 *Commun. Math. Phys.* **9** 267
[19] Luijten E and Blöte H W 1997 *J. Phys. Rev.* B **56** 8945
[20] Nelson D R and Fisher M E 1975 *Ann. Phys.* **91** 226
[21] Abramowitz M and Stegun I A 1965 *Handbook of Mathematical Functions* (New York: Dover)
[22] Cardy J L 1981 *J. Phys. A: Math. Gen.* **14** 1407
[23] Luijten E and Meßingfeld H 2001 *Phys. Rev. Lett.* **86** 5305
[24] Antal T, Droz M and Rácz Z 2004 *J. Phys. A: Math. Gen.* **37** 1465
[25] Köfinger J 2009 *Water in Nanopores* (Vienna: University of Vienna) http://othes.univie.ac.at/4514/
[26] Patria R K 1972 *Statistical Mechanics* (Oxford: Butterworth-Heinemann)
[27] McQuarrie D A 2000 *Statistical Mechanics* 2nd edn (New York: University Science Books)
[28] Vaitheeswaran S, Rasaiah J C and Hummer G 2004 *J. Chem. Phys.* **121** 7955
[29] Koga K, Gao G T, Tanaka H and Zeng X C 2001 *Nature* **412** 802
[30] Maniwa Y, Kataura H, Abe M, Udaka A, Suzuki S, Achiba Y, Kira H, Matsuda K, Kadowaki H and Okabe Y 2005 *Chem. Phys. Lett.* **401** 534
[31] Mikami F, Matsuda K, Kataura H and Maniwa H 2009 *ACS Nano* **3** 1279
[32] Chaban V 2010 *Chem. Phys. Lett.* **496** 50–5
[33] Saha S K and Chakravorty D 2006 *Appl. Phys. Lett.* **89** 043117
[34] Matyushov D V 2007 *J. Chem. Phys.* **127** 054702
[35] Menzl G, Köfinger J and Dellago C unpublished work